symmetry

MDPI

Article

The Influence of Low-Frequency Oscillations on Trailing-Edge Tonal Noise with Symmetry Spanwise Source Regions

Zhangchen Song [1], Peiqing Liu [1], Hao Guo [1,*], Yifeng Sun [2] and Shujie Jiang [3]

[1] School of Aeronautic Science and Engineering, Beihang University, Beijing 100191, China; songdbs_work@buaa.edu.cn (Z.S.); lpq@buaa.edu.cn (P.L.)
[2] COMAC Shanghai Aircraft Design and Research Institute, Shanghai 201315, China; sunyifeng@comac.cc
[3] Laboratory of Aerodynamic Noise Control, China Aerodynamics Research and Development Center, Mianyang 621000, China; anjsj@126.com
* Correspondence: guohao@buaa.edu.cn; Tel.: +86-135-1106-0706

Abstract: For noise reduction at a low-to-moderate Reynolds number, airfoil trailing-edge tonal noise has multiple prominent tones. Among these tones, secondary tones are greatly influenced by external disturbances such as oscillations commonly in the environment. In previous experiments, the spatial movement of sources was found to be related to an inherent high-frequency oscillation. Therefore, the spatial influence of external low-frequency oscillations was investigated in this study. By using tripping tapes to construct different symmetry source regions on the pressure side with side secondary tones, a transient spatial analysis of an NACA0012 airfoil at 2 degrees was performed by microphone arrays when a 10 Hz pressure oscillation was significant at 24 m/s. Temporally, this 10 Hz periodic strength change became more intense at a broader frequency bandwidth for a longer source region. Furthermore, a substantial time delay, significantly larger than the sound propagating time difference between microphones, was observed exclusively along the spanwise direction. This delay led to a periodic directivity pattern, particularly when two 0.2 m source regions were separated by a 0.2 m or 0.4 m tripping region. This low-frequency oscillation introduces an asymmetric transient switching pattern for symmetric spanwise source regions. Consequently, the response of airfoils to external oscillations in field tests should be considered.

Keywords: aeroacoustics; microphone array; transient analysis; low-frequency oscillation

check for updates

Citation: Song, Z.; Liu, P.; Guo, H.; Sun, Y.; Jiang, S. The Influence of Low-Frequency Oscillations on Trailing-Edge Tonal Noise with Symmetry Spanwise Source Regions. *Symmetry* **2024**, *16*, 710. https://doi.org/10.3390/sym16060710

Academic Editor: Zine El Abiddine Fellah

Received: 7 May 2024
Revised: 27 May 2024
Accepted: 29 May 2024
Published: 7 June 2024

Copyright: © 2024 by the authors. Licensee MDPI, Basel, Switzerland. This article is an open access article distributed under the terms and conditions of the Creative Commons Attribution (CC BY) license (https://creativecommons.org/licenses/by/4.0/).

1. Introduction

Aerodynamic noise has been an unignorable factor for engineering applications such as unmanned aerial vehicles and small wind turbines at a low-to-moderate Reynolds number [1–3]. Among these noises, airfoil noise is of great importance and is directly related to aerodynamic performance, which is critical in quiet airfoil designs [4–6]. Among these airfoil self-noises, airfoil trailing-edge tonal noise is so prominent that scientists all over the world have spent decades conducting experiments and simulations to understand the noise and noise reduction mechanism [7–29]. Generally, at a moderate Reynolds number between $Re_c = 2 \times 10^4$ and $Re_c = 2 \times 10^6$, this noise has one or several narrowband tones and some broadband humps in the acoustic spectra [20]. Due to the influence of the acoustic feedback loop (AFL) and the flow instability growth in noise amplification, the frequency of the multiple tones has a piecewise ladder structure with jumps at certain velocity ranges [16]. The dominant tone is related to the steady periodic symmetric shedding vortical structures along the spanwise direction, while the secondary tones are attributed to the intermittent unsymmetric changes in the frequency, time and spatial domains [23]. As a result, interesting transient patterns related to secondary tones have been found, such as switching tones [19,24], side secondary tones [21] and the periodic spanwise movement of sources [22]. Meanwhile, the difference between experiments and simulations [19] has attracted researchers to analyze the occurrence of transient patterns in spatial distributions.

Hence, it is of great significance to investigate trailing-edge tonal noise in the frequency, time and spatial domains.

Basically, according to Longhouse [10], trailing-edge tonal noise began as an initial disturbance on the transitional region, which grew in the boundary layer towards the trailing edge, scattering as shedding vortical structures around the edge to release acoustic waves backward, causing new initial disturbances that propagate forward and maintain a phase-match state. In this process, AFL dominated the selection of amplificated tones on the broadband hump from growing instabilities along the airfoil, which produced corresponding flow coherent structures. In experiments based on the transient correlation analysis between velocity signals from particle image velocity (PIV) data and acoustic signals from a single microphone, Pröbsting [15] confirmed that the vortical structures shed at the same frequency as the dominant tone frequency. And the growing instabilities were the result of Tollmien–Schlichting (T-S) instability along the boundary layer [15] and Kelvin–Helmholtz (K-H) instability related to the laminar separation bubbles [17]. In simulations, Ricciardi [23] found that although the AFL confirmed that only a dominant tone existed during the initial cycles, secondary tones would gradually emerge due to the unsteadiness of growing instabilities after several cycles. In addition, scientists pointed out that the strength of noise sources in the time domain was receptive to the pressure oscillations [13] and dynamics of flow coherent structures [23,25]. Furthermore, experiments confirmed that trailing-edge tonal noise was sensitive to external disturbances from a surface-mounted plasma actuator [30], acoustic excitation [31] and serrations [32]. Therefore, as an inevitable disturbance in the open test section from the wind tunnel buffeting [33], the low-frequency pressure oscillation should be considered in the transient source localization of trailing-edge noise measurement.

In the literature, this low-frequency pressure oscillation generally exists in the open test section of low-speed wind tunnels [33,34]. It usually has a frequency lower than 20 Hz accompanied by velocity fluctuations [35,36]. Called wind tunnel buffeting, pumping or swaying in the literature [37–40], this phenomenon is generally attributed to a feedback loop between the shear layers around the inlet nozzle and flows around the collector through the coherent vortex structures [34]. Consequently, since trailing-edge tonal noise is receptive to the flow of coherent structures [41], it is possible for the low-frequency pressure fluctuation in the flow to influence the trailing-edge tonal noise in the frequency, time and spatial domains.

According to the amplitude modulation theory [42], a periodic strength change can produce side tones around the dominant tone in equal frequency intervals. In experiments, Pröbsting [15] confirmed that this periodic modulation of the fluctuation amplitude in the vortical structures on one side of the airfoil could produce secondary tones. In simulations, Ricciardi [23] concluded that the different periodic changes in spanwise coherence led to different secondary tones. Specifically, for airfoil trailing-edge tonal noise, when the coherent flow structure passes the airfoil edge, a spatial–temporal unsteady pattern influenced the amplitude of the dominant tone and produced secondary tones. Hence, based on the results of experiments and simulations by the transient wavelet analysis between acoustic fields and velocity fields, the emergence of secondary tones is a result of the periodic and intermittent coherent flow structures [15,17,23,24]. Correspondingly, according to Yang's PIV measurement experiments with proper orthogonal decomposition (POD) [21], low-frequency oscillations beneath the incoming flow produced the side secondary tones at a frequency gap lower than 20 Hz. In addition, similar patterns could be found due to forced disturbances in the literature [30–32]. Therefore, being influenced by the low-frequency pressure oscillation, the source region should have a spatial transient source distribution pattern, which awaits further experiments.

In source localization problems, the microphone array technique has been widely used in experiments [43–46]. It utilizes the difference of time in propagating between microphones to localize sources. In recent years, thanks to the development of wavelet-based beamforming methods [47–49], it is possible for airfoil experiments to investigate transient

source localization. It was found by Yu [22] that the major noise sources moved along the spanwise direction at a frequency according to the amplitude modulation frequency. Hence, if the low-frequency oscillations changed the dominant tone's strength in a similar way, there could be an obvious transient spatial movement pattern due to the long period time of the low frequency. Since the deformations of airfoils and unsteady flow oscillations might exist at a low frequency for UAVs and wind turbines in the environment, this response to the external oscillations from the environment should be considered in airfoil design if the results show significant patterns.

In this study, aimed at investigating the influence of low-frequency oscillation on trailing-edge tonal noise in the frequency, time and spatial domains, two microphone arrays were introduced to localize sources on different specially designed spanwise source regions of an NACA0012 airfoil model. This airfoil had a chord length of 0.1 m and a span of 1.6 m on the open test section of the Beihang D5 aeroacoustics wind tunnel [50]. The reason to choose an NACA0012 profile is due to the existing large number of trailing-edge tonal noise investigations based on NACA0012 with different chord lengths and spans [4,7,11,12,15,19,22]. NACA0012 shows a steady time-average pattern within a considerable velocity range, which makes it credible to highlight the influence of the flow oscillations. For the currently open test section of a D5 aeroacoustics wind tunnel, a 10 Hz strong oscillation due to wind tunnel buffeting could be found at 24 m/s according to the background noise measurement, which was able to produce a strong periodic strength change in the time domain. To further highlight the role of this low-frequency pressure oscillation on the noise signals, the tripping tapes on the airfoil suction side diminished the phase modulation between flow structures from two sides of the airfoil [13], and cases with high-frequency intervals for primary secondary tones were excluded. Therefore, different configurations for symmetry spanwise distributions of source regions could be created on the pressure side, where only one dominant tone with only side secondary tones due to the 10 Hz oscillation was present.

Inspired by the previous experiments in localizing transient sources [22], microphone arrays were employed with wavelet-based beamforming methods. Based on the 64-channel spiraled microphone array, source strength distribution maps in a high spatial resolution were generated to validate the time-average consistent pattern along the spanwise direction. Based on the 21-channel cross-shaped microphone array, simultaneous acoustic measurement along the spanwise direction and horizontal direction could be achieved to analyze the different transient patterns along the spanwise and horizontal directions directly. By using continuous wavelet analysis and a corresponding wavelet-based beamforming method, periodic strength changes in the frequency, time and spatial domains were detected. According to the transient source strength distribution maps, the symmetry source region along the spanwise direction produced a switching pattern between consecutive line sources and separated sources in the time domain. During this periodic switching process, unsymmetric strength distributions were found along the spanwise direction for each microphone as a periodic directivity pattern. It was found that a significant large time delay between microphones only along the spanwise direction was responsible for the periodic directivity pattern. Hence, the response to the low-frequency oscillations in the flow field became a significant characteristic. For future airfoil designs involved with trailing-edge tonal noise, the noise measurement experiments should consider the airfoil's response to environmental disturbances.

The structure of this paper is as follows: Section 2 will briefly introduce the flow facility, experiment setup and analysis tools. The configurations with different spanwise source regions will be illustrated in diagrams, and beamforming methods will be discussed. Section 3 is concerned with the results of the time-average, transient and spatial–temporal analyses. The time-average characteristics, such as the ladder structure of tonal frequencies and spatial distribution of sound sources, will be illustrated in plots and contour maps. The strong 10 Hz oscillation at 24 m/s was first proposed in the background noise measurement. Then came the time-average analysis for the trailing-edge noise validation in the frequency

and spatial domains. Transient analysis by continuous wavelet transform was performed to evaluate the difference between different spanwise distributions of source regions. For cases with a 0.2 m tripping region inside the symmetry 0.6 m source region, it was found that the 10 Hz oscillation had a significant time delay between different microphones only along the spanwise directions, which contributed to a switching pattern between consecutive strong line sources and weak separated sources. In contrast, the microphones along the horizontal direction showed consistent results in the time delay. As a result, by decreasing the horizontal microphones' weight in the calculation, nearly equal strength of sources for two types of source strength distribution could be achieved at the cost of a low horizontal resolution.

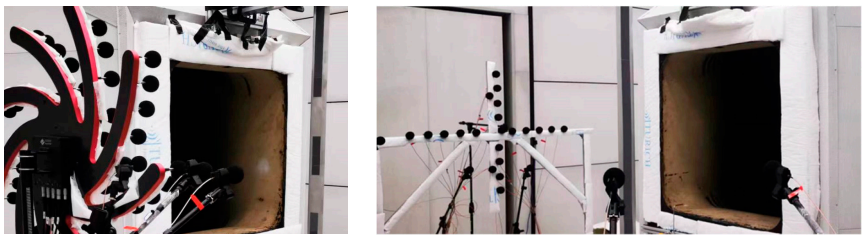
2. Materials and Methods

2.1. Experiment Setup

The experiment for the trailing-edge tonal noise investigation was conducted at the Beihang D5 aeroacoustics wind tunnel [50] at Beihang University. The D5 wind tunnel is a small-scale, closed-circuit wind tunnel with a cross-section of 1 m $\times$ 1 m (height $\times$ width). The length of the open test section is 2 m from the nozzle to the collector.

The airfoil is an aluminum 0.1 m chord length NACA0012 with a sharp trailing edge (around 0.2 mm at height). It has a span of 1.6 m, which is long enough to cover the shear layer length and leave enough spanwise source region within the uniform flow from the nozzle. The airfoil is placed vertically with a sweep angle of less than 0.5 degrees according to a laser level. The suction side of the airfoil is fully tripped by coarse tapes (the tape has a height of 0.5 mm). In this study, the angle of attack is fixed at 2 degrees and the incoming flow velocity ranges from 10 m/s to 60 m/s.

For noise measurement, a 64-channel spiraled microphone array and a 21-channel cross-shaped microphone array were placed at a distance of 1.5 m toward the pressure side of the airfoil in two separate experiments with the same model setup. As shown in Figure 1, general views in experiments are presented for these two microphone arrays with the airfoil. Specifically, a geometry placement between the airfoil and arrays is shown in Figure 2. Both the centers of these arrays were placed towards the symmetry line of the trailing edge. For the cross-shaped microphone array, 11 microphones are in the same horizontal line, and 9 microphones are in the same spanwise line vertically.



(**a**) (**b**)

Figure 1. The experiment setups of (**a**) the 64-channel spiraled microphone array in a view from pressure side of the airfoil, and (**b**) the 21-channel cross-shaped microphone array in a view from the suction side of the airfoil. The suction side surface of the airfoil is fully tripped.

GRAS 40PH (GRAS Sound & Vibration from Holte, Denmark) and Brüel & Kjær 4954A (Hottinger Brüel & Kjær from Hertfordshire, UK) microphones with a sampling rate of 51,200 Hz for a duration of 30 s were applied for the 64-channel spiraled array and the 21-channel cross-shaped array, respectively. They are both high-accuracy free-field microphones and calibrated under the same GRAS 42AA pistonphone (GRAS Sound & Vibration from Holte, Denmark). An average periodogram method was used to generate estimates of the power spectrum density (PSD) and sound pressure level (SPL). For the general time-average analysis, the number of samples per window was 12,800, resulting in a frequency resolution of 4 Hz. For the low-frequency oscillation analysis and auto-spectrum

of wavelet power coefficients, each window block consisted of 102,400 samples, which contributed to a frequency resolution of 0.5 Hz. The Hanning window and an overlap of 50% were applied in the analysis.

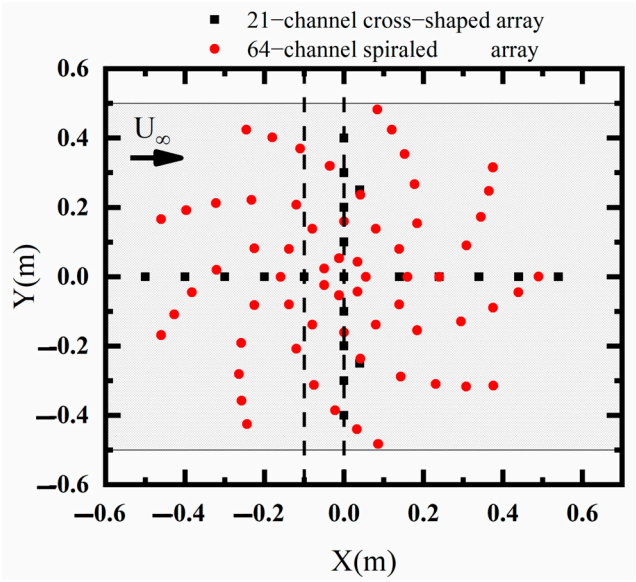


Figure 2. The geometry position of arrays with microphones and airfoils in the X-Y plane. The dashed black lines indicate the leading edge and trailing edge of the airfoil on the left and on the right, respectively. The black squares refer to the BK 4189A microphones for the 21-channel cross-shaped array, while the red circles refer to the GRAS 40PH microphones for the 64-channel spiraled array. The incoming flow direction is highlighted by the arrow.

As previously shown in Figure 1, the suction side was fully tripped, while the pressure side was tripped partially to create different source regions. In this study, the main configurations are shown in Figure 3 with different spanwise conditions on the pressure side. A set of terms, such as *L*0, *L*2 and *L*8*T*4, are defined according to the lengths of the clean region and tripped region. The number after *L* refers to the length of clean regions in a unit of 0.1 m, and the number after *T* stands for the length of the tripping region within the clean region in a unit of 0.1 m. Three dotted square lines are used to further distinguish configurations in different clusters. For configurations within region (a) and region (b), a symmetry placement of clean regions is present. Configurations within region (c) are aimed at evaluating the time-average consistency along the spanwise direction. Hence, an additional microphone was positioned on the pressure side towards the center of the 0.2 m clean region at a distance of 1.2 m as the reference microphone. For other cases, the reference microphone from the microphone arrays was positioned on the pressure side towards the center of the airfoil trailing edge within the uniform flow region at a distance of 1.5 m.

2.2. Microphone Array Methods

In comparison with the velocity measurement from invasive hotwires and short-time-period particle image velocity (PIV) in the flow field, the microphone array method is non-invasive and can obtain long-time-period data [43]. By using wavelet-based beamforming methods [22], it is possible to describe the high-correlated flow-induced noise sources in the time and spatial domains, especially when the spanwise source strength distribution is inconsistent due to tripping devices.

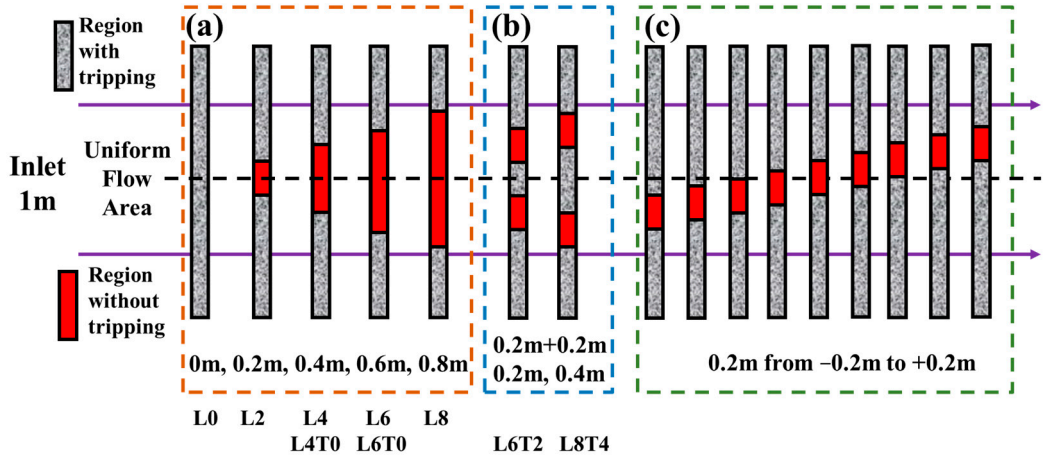


Figure 3. The surface conditions of the pressure side of airfoils for different configurations. The red filled area indicates the source region without tripping. The grey shadow area indicates the region with tripping. (**a**) Fully tripped region or source regions in consistent symmetrical distributions. (**b**) A disruption of tripped region between source regions. (**c**) Different locations of the 0.2 m clean region. The incoming flow has a spanwise length of 1 m. Without T, L stands for the length of symmetry clean region without tripping. T refers to the length of symmetric tripping region inside clean regions from L.

For source localizations by microphone array, a brief introduction of the beamforming method and the wavelet beamforming method are illustrated below. A detailed discussion of different microphone array methods can be found in a review [51]. According to the delay-and-sum approach, the estimated spatial strength distributions of sound sources are deduced by the microphones' time signals and the spatial distributions between scanning points and microphones. The sound pressure at a scanning position $\vec{x}_b$ is deduced in Equations (1) and (2) in the time and frequency domain, respectively.

$$bf\left(\vec{x}_b, t\right) = \frac{1}{M}\sum_{m=1}^{M} w_m A_m\left(\vec{x}_b, \vec{x}_m\right) p_m\left(t - \frac{\left|\vec{x}_b - \vec{x}_m\right|}{c}\right) \tag{1}$$

$$bf\left(\vec{x}_b, \omega\right) = \frac{1}{M}\sum_{m=1}^{M} w_m A_m\left(\vec{x}_b, \vec{x}_m\right) p_m(\omega) e^{j\omega\frac{\left|\vec{x}_b - \vec{x}_m\right|}{c}} \tag{2}$$

$$p_m(\omega) = \frac{1}{t_2 - t_1}\int_{t_1}^{t_2} p_m(t) e^{j\omega t} dt \tag{3}$$

In these equations, the following apply:

- t is global time and $\omega(= 2\pi f)$ is the angular frequency for the Fourier transform;
- p_m is the sound pressure signal for the number m microphone. In the time domain, $p_m(t)$ is the transient sound pressure according to the global time. In the frequency domain, $p_m(\omega)$ represents the estimated complex strength and phase in a frequency for a time period ranging from t_1 to t_2. By confining the value of $t_2 - t_1$, a relatively transient estimation of sound source is achieved in the frequency domain;
- $\vec{x}_m$ is the position of the number m microphone;
- w_m is a weight function to determine the influence of the number m microphone;
- $A_m\left(\vec{x}_b, \vec{x}_m\right)$ is the propagating scale factor to determine the decaying of signal strength according to the distance between the microphone and the sound source. For the monopole point source and Green function, $A_m\left(\vec{x}_b, \vec{x}_m\right) = \frac{1}{4\pi\left|\vec{x}_b - \vec{x}_m\right|}$.

By using the short-term Fourier transform and defining the length of the time period, an estimation of source positions in different frequencies is produced in a relatively large time resolution. And by averaging over the time periods, a typical time-average conventional frequency domain beamforming result can be produced. In the current experiments, the maximum time delay between each microphone should be below 0.002 s, which is much less than the 10 Hz time period of 0.1 s.

Analogously, by substituting continuous wavelet transform from the Fourier transform in Equation (3), a high-time-resolution time domain microphone array method can be produced as the wavelet-based beamforming method. In the literature [22,47–49], the wavelet-based beamforming methods showed extraordinary abilities in detecting the movement of sources, identifying the relative strength shift between sources and increasing the signal-to-noise ratio to perform better cross−correlation analysis. In this paper, complex Morlet wavelets are applied to acquire the temporal phase information. The selection of an appropriate non-dimensional frequency and other parameters has been undertaken to better describe the spatial and time characteristics. And a source integration method [52,53] is introduced to calculate summed SPL over different source regions. For the spanwise source regions, the calculated horizontal regions cover a whole chord length (0.1 m) from the center of the airfoil toward the trailing edge.

3. Results

3.1. Time-Average Analysis

As has been mentioned in the introduction, low-frequency pressure oscillations commonly exist in wind tunnel experiments [34]. For the open test section of the Beihang D5 aeroacoustics wind tunnel, strong pressure oscillations can be detected through background noise measurement. As shown in Figure 4, a contour map of PSD for the background noise is produced within a velocity range from 10 m/s to 60 m/s. The constant tone at 4 Hz is related to the inherent natural frequency of the anechoic chamber. The tone changing at different velocities is a result of the unsteady coherent vortices in the shear layer. For example, a dashed line indicates a velocity-dependent frequency law between the wind tunnel's inner frequency and incoming flow velocity as $f = 0.2U + 5.2$ in standard science units. Among these tones, the significantly strong tone is a result of amplification due to resonance between the nozzle and collector, which contributes to the well-known wind tunnel buffeting phenomenon [35]. The dashed line and dotted line in Figure 4 indicate a strong 10 Hz oscillation around 24 m/s, which is focused on in the present study as it is the strong low-frequency pressure oscillation that influences the trailing-edge tonal noise.

In order to validate the airfoil trailing-edge noise and check if the tripping tapes succeed in having only pressure side sources, a series of acoustic measurements has been performed for configuration $L2$ and $L0$ at different incoming flow velocities. The angle of attack is fixed at 2 degrees, so the upper surface is the suction side and the down surface is the pressure side towards the reference microphones. The time-average PSD by the reference microphone from the 64-channel microphone array is presented in contour maps and plots in Figure 5. In Figure 5a, ladder-type structures are indicated by black dashed lines with jumps. The dominant tones are highlighted by red cycles whose frequencies follow a 0.85th power law of velocity on ladders with a jump between different ladders. During a velocity range from 18 m/s to 28 m/s, no primary secondary tones are found in a high frequency interval around the dominant tones. Specifically, for cases ranging from 20 m/s to 28 m/s at an interval of 2 m/s, the dominant tones in Figure 5b are significantly stronger than the fully tripped broadband noise. In general, the time-average noise power spectra have validated the airfoil trailing-edge tonal noise experiments with the suction side being fully tripped among all the other experiments in the literature [7,11,16]. In addition, the 10 Hz oscillation has been found in Figure 5c at 24 m/s and 26 m/s for configuration $L2$ and $L0$, which will be focused on in the following transient analysis.

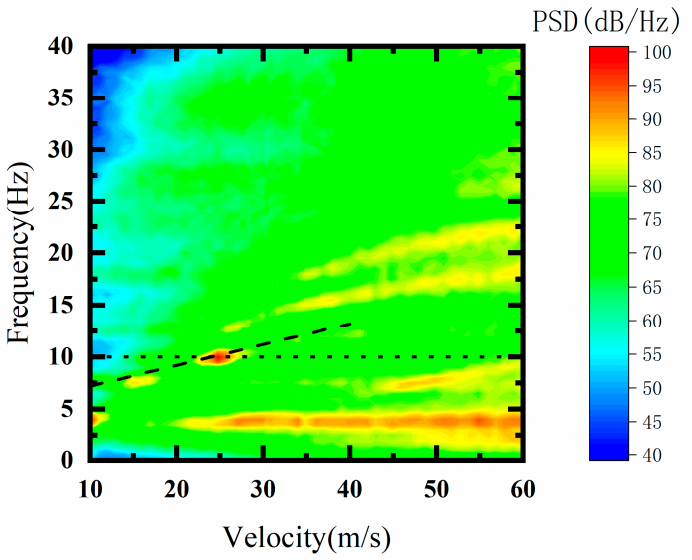


Figure 4. A contour map of acoustic spectra of PSD for the background noise. Without the airfoil within the flow regions, the background noise is measured by the reference microphone at a distance of 1.5 m towards the centerline of the open test section. The dashed line is an approximate line as $f = 0.2U + 5.2$ for low-frequency oscillations with a 10 Hz peak at 24 m/s. The dotted line indicates the 10 Hz oscillation.

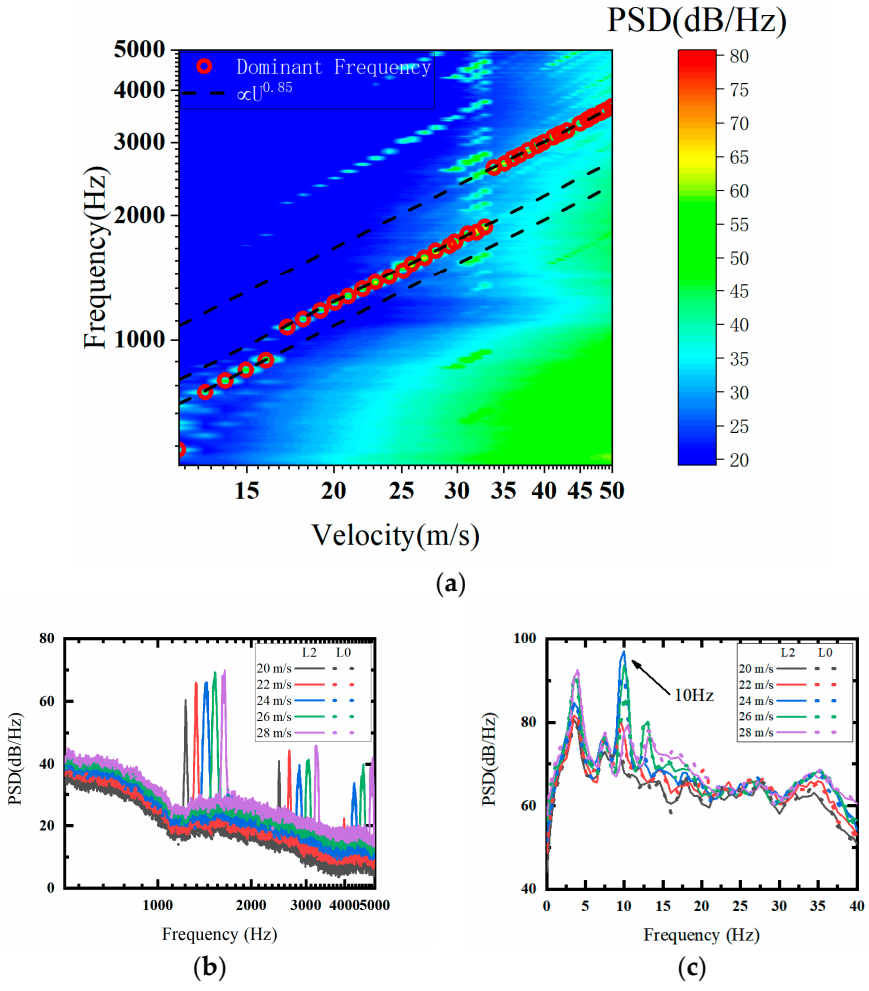


Figure 5. The time-average noise characteristics according to the reference microphone from the 64-channel spiraled array. (**a**) A contour map of acoustic spectra of PSD for the configuration *L*2 with

incoming flow velocities ranging from 10 m/s to 50 m/s; (**b**) plots of PSD ranging from 20 m/s to 28 m/s for the configuration $L2$ and $L0$. $L2$ is the straight line and $L0$ is the dotted line; (**c**) zoomed plots of (**b**) in a low frequency range. The 10 Hz oscillations at 24 m/s and 26 m/s are highlighted by an arrow.

In order to exclude the inherent influence on different spanwise configurations, an evaluation of the spanwise consistency was performed by moving the 0.2 m source region in a spanwise range from $z = -0.2$ m to $z = 0.2$ m in Figure 3c. A moving microphone towards the center of the 0.2 m source region and the 64−channel spiraled microphone array were used to compare the time-average characteristic in the frequency–spatial domains. As shown in Figure 6, contour maps of PSD for the moving microphone towards different spanwise locations of the source region were present at a velocity range from 20 m/s to 28 m/s. Due to the velocity fluctuations, a difference in dominant tone frequency occurs, but a generally similar pattern was confirmed along the spanwise directions. As shown in Figure 7, time-average source localization of the 0.2 source region at different spanwise locations validated that the tripping tapes confined the sound sources within the 0.2 m clean region and there was a similar spatial pattern along the spanwise direction. SPL was summed at a 1/3 octave around the center frequency of 1424 Hz.

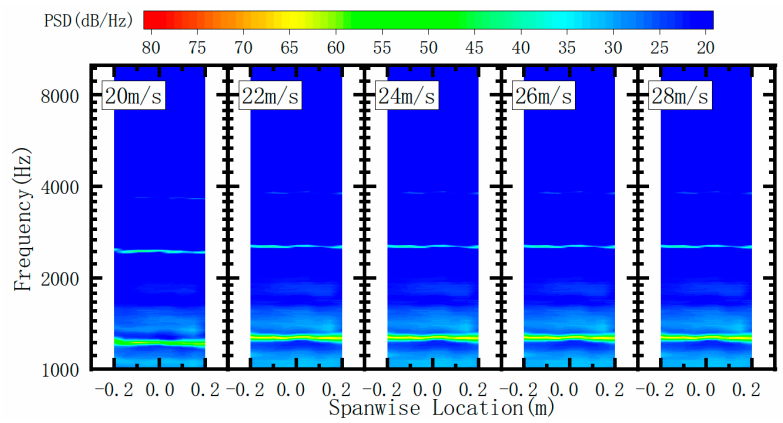


Figure 6. The time-average PSD for the moving 0.2 m clean region along the spanwise location at different velocities according to the moving microphone. The moving microphone is placed towards the center of 0.2 m clean region at a fixed distance of 1.2 m.

Based on the results of source localization and strength measurement for the 0.2 m source region, a symmetric source distribution should be present for a symmetric source region in source localization. As shown in Figure 8, the time-average source localization maps at 24 m/s for different spanwise configurations show a generally symmetric source strength distribution, especially for the configuration $L6$. SPL is summed at a 1/3 octave around the center frequency of 1424 Hz, which is enough to consider the frequency deviation along the spanwise direction. In addition, a spurious source was found in the tripping region for the configuration $L6T2$ in comparison with $L6$. According to the spatial resolution of beamforming methods established from the Rayleigh limit [43], the spurious source is attributed to the insufficient distance between two symmetric 0.2 m source regions. Proof is given in Figure 9 as source localization maps, where two 0.2 m source regions are measured independently with a sum of the strength of the two source localization maps. The source strength distribution map in Figure 8e is similar to the one in Figure 9c. Therefore, it could be assumed that the impact of the low-frequency pressure oscillation on the time-average result of the summed SPL over a wide frequency range is insignificant. However, in the following transient analysis with a better frequency-time resolution, the influence of the low-frequency oscillation becomes notable.

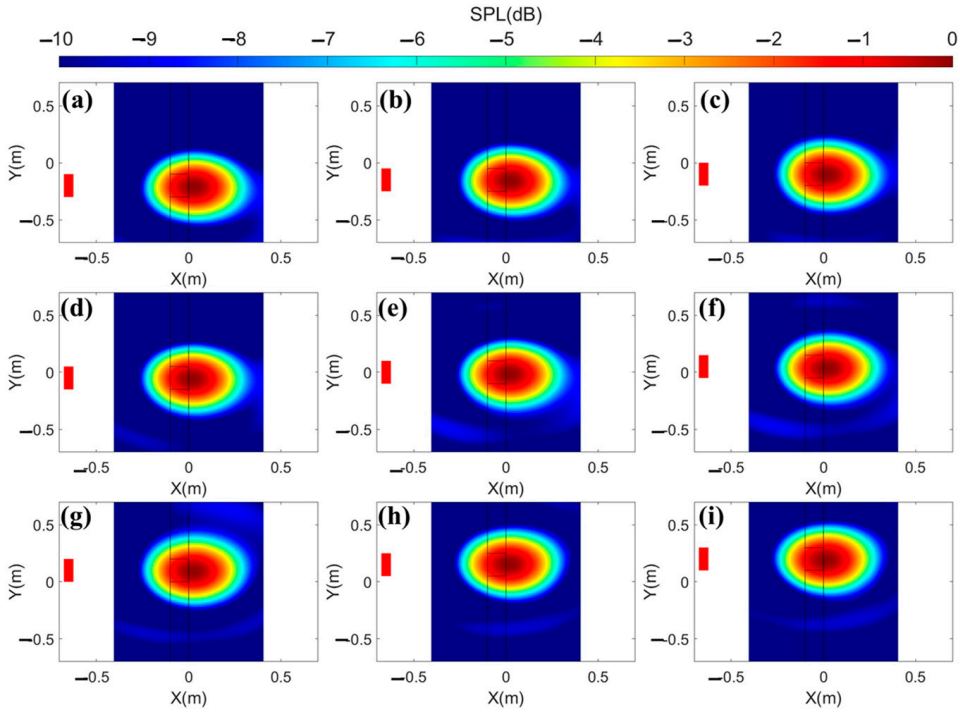


Figure 7. The time-average source localization for the moving 0.2 m clean region along the spanwise location at 24 m/s according to the 64-channel spiraled microphone array. (**a**–**i**) refer to the spanwise location from $z = -0.2$ m and $z = 0.2$ m in Figure 6. The black X−direction lines refer to the leading edge and trailing edge, while the black Y-direction lines indicate the red source regions on the left.

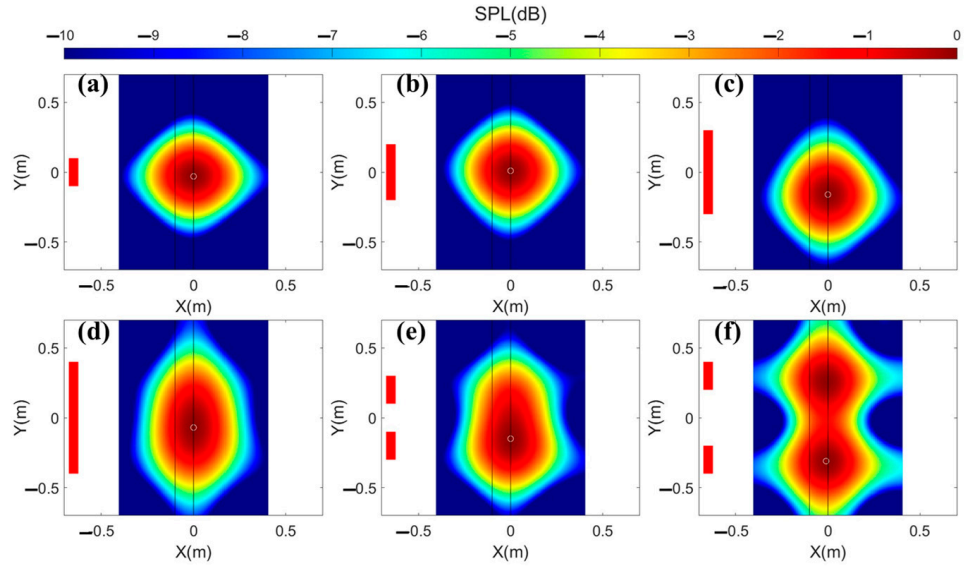


Figure 8. The time-average source localization of different source regions along the spanwise location at 24 m/s according to the 21-channel cross-shaped microphone array. (**a**) *L*2; (**b**) *L*4; (**c**) *L*6; (**d**) *L*8; (**e**) *L*6*T*2; (**f**) *L*8*T*4. The black lines refer to the leading edge and trailing edge. The unfilled white cycles indicate the positions of maximum SPL, which is located around the trailing edge.

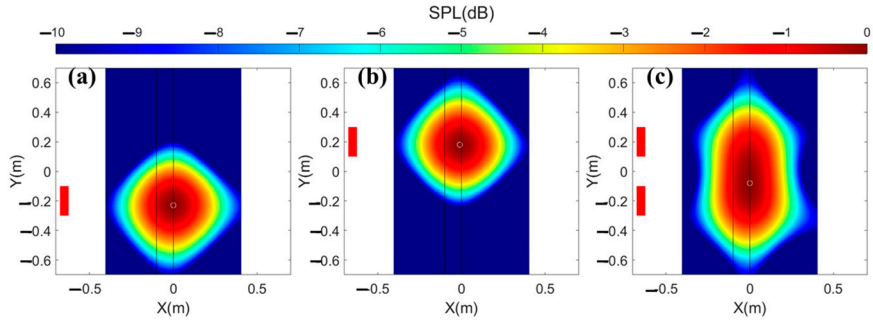


Figure 9. The time-average source localization of different source regions along the spanwise location at 24 m/s according to the 21-channel cross-shaped microphone array. (**a**) The 0.2 m source region in the down part; (**b**) 0.2 m source region in the upper part; (**c**) a sum of (**a**,**b**) to produce *L*6*T*2. The black lines refer to the leading edge and trailing edge. The unfilled white cycles indicate the positions of maximum SPL, which is located around the trailing edge.

3.2. Transient Analysis

By using continuous wavelet analysis, the transient characteristics of noise signals can be revealed. As a time-frequency-dependent parameter, the wavelet coefficient W stands for the transient efficient amplitude at a certain frequency. W_n^2 is defined as a non-dimensional normalization of the square absolute values of the wavelet coefficient W according to the maximum values in the contour maps. The reference microphone at the symmetrical line towards the airfoil trailing edge is chosen to compare the transient results between different spanwise configurations at 24 m/s.

As shown in Figure 10, a periodic 10 Hz strength change around the dominant tone could be found in the frequency-time domain, especially for configurations *L*2 and *L*4. Therefore, according to amplitude modulation, side secondary tones should be present in the time-average acoustic spectra, which are present in Figure 11. The black square and red cycle symbols indicated a 10 Hz interval, which was similar to the side secondary tones' pattern in the literature [21]. Meanwhile, as shown in Figure 10, a larger spanwise length of the source region (from *L*4 to *L*8) can greatly increase the unsteadiness towards a higher value in the time domain. For *L*6*T*2 and *L*8*T*4, a decrease in clean regions by adding tripping tapes inside the total spanwise clean region tends to control the periodic strength change in a much more regular and steady way.

Moreover, by using an auto-spectrum of the total strength around the center frequency (1424 Hz at 24 m/s) in a 1/3 octave way, the 10 Hz oscillations were prominent as peaks for all configurations in Figure 12. From *L*2 to *L*8, an increase in the total spanwise source regions led to a larger sound strength in a more broadband-like way. While *L*2 and *L*4 mainly show the 10 Hz peak and 20 Hz harmonic peak, a tendency of larger frequency oscillation can be observed in *L*6 and *L*8. When tripping regions were added, *L*6*T*2 and *L*8*T*4 were degenerations of *L*6 and *L*8 in strength and regularized in the time domain. In addition, the normalization of the auto-spectrum strength as $E(f)/E(0)$ clearly exhibited this similar normalization pattern at 10 Hz. The tripping region within the clean region increased the quality factors of the dominant tone and decreased the lower frequency broadband components.

Similar to previous experiments in the literature [21], by transient analysis, a periodic strength change in the dominant tone was confirmed with the 10 Hz oscillation to produce side secondary tones. Therefore, it is feasible to carry on spatial–temporal analysis for the influence of low-frequency oscillation on trailing-edge tonal noise. Based on the above transient results for the single reference microphone, the procedure to compare different microphones in the horizontal line and spanwise line can be performed, and transient source localization by the wavelet beamforming method could be undertaken.

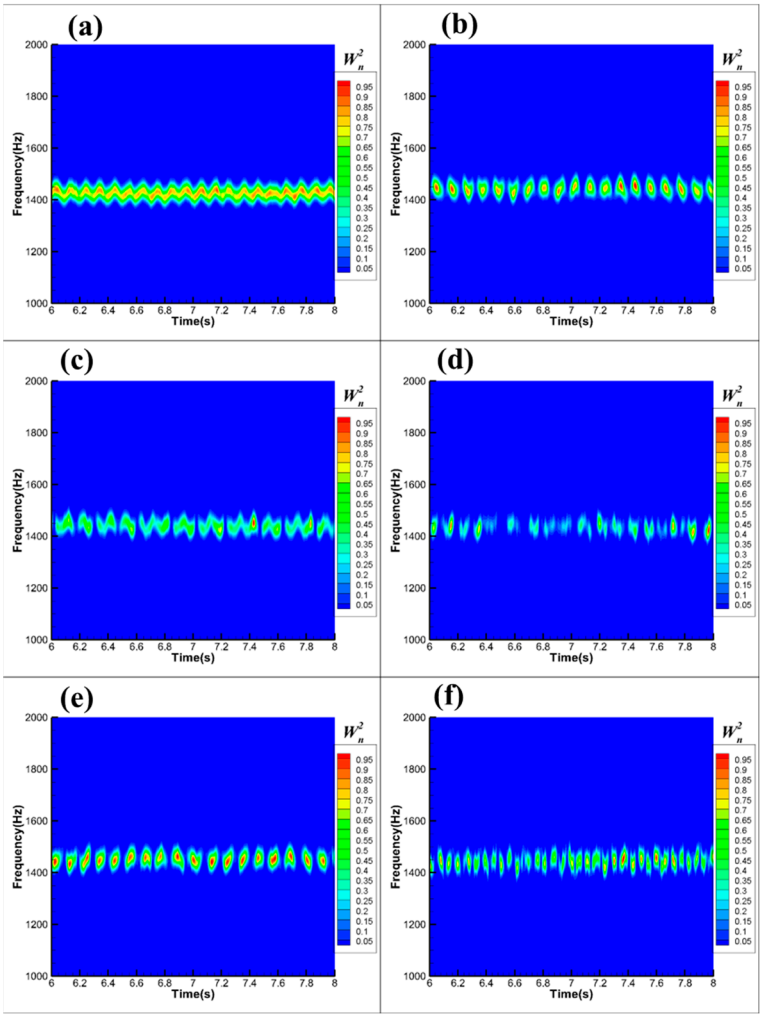


Figure 10. The normalized wavelet coefficients in contour maps for different spanwise configurations. The incoming velocity is 24 m/s. (**a**) *L*2; (**b**) *L*4; (**c**) *L*6; (**d**) *L*8; (**e**) *L*6*T*2; (**f**) *L*8*T*4.

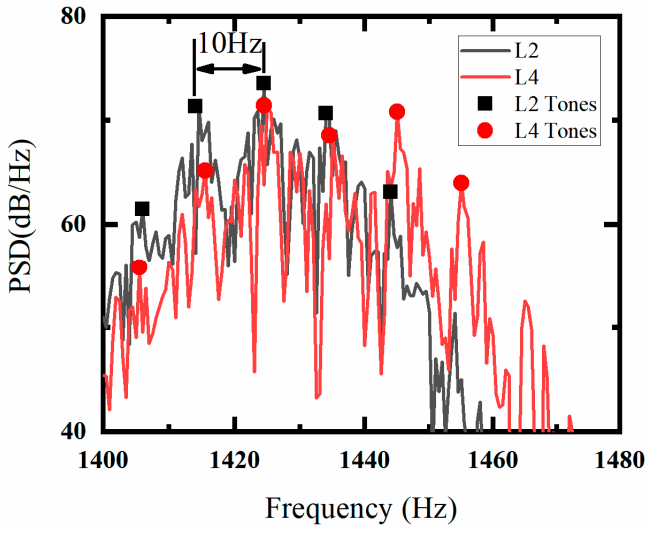


Figure 11. The time-average PSD according to the reference microphone from the 21-channel cross-shaped array for *L*2 and *L*4 at 24 m/s. A sampling time from 6 s to 8 s is applied as in Figure 9. A 10 Hz interval could be found between tones. The square black symbols refer to tones for *L*2, while the red cycle symbols refer to tones for *L*4.

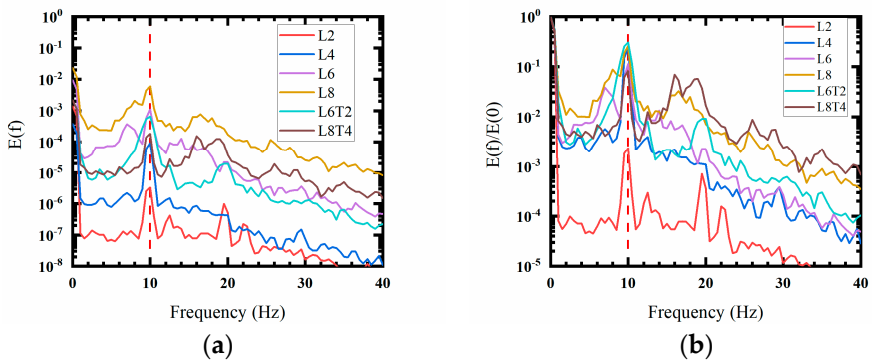


Figure 12. (**a**) Auto-spectrum of the summed wavelet coefficients around the dominant tone frequency in a 1/3 octave for different spanwise configurations at 24 m/s; (**b**) normalization of the auto-spectrum from $E(f)$ to $E(f)/E(0)$. Dashed red lines indicate 10 Hz peaks.

3.3. Spatial–Temporal Analysis

To address the influence of intermittency in the time and spatial domains, the transient results of microphones at different locations are compared. According to the spatial distribution of the 21-channel cross-shaped microphone array in Figure 2, microphones from the 21-channel microphone array can be divided into two parts along the horizontal and spanwise locations, respectively. By using the same wavelet analysis process in Section 3.2, the SPL is summed from the center frequency (1424 Hz at 24 m/s) in a 1/3 octave frequency range. The results of the SPL for microphones along horizontal and spanwise directions are shown in Figures 13 and 14, respectively.

As shown in Figure 13, the microphones at horizontal locations reveal a consistent periodic strength change pattern in the time domains for all configurations from *L*2 to *L*8. Although an increased length generates a more complicated pattern in the time domain, the strengths along the horizontal line remain identical in the time domain. In contrast, in Figure 14, the microphones along the spanwise direction indicate an unsteady, uneven time delay for the low-frequency oscillation. As has been mentioned in Section 2.2 about the microphone array methods, the maximum time delay between microphones in current experiments should not exceed 0.002 s, which is much less than the delay time period in Figure 14 between horizontal microphones for *L*6*T*2 and *L*8*T*4. In comparison, a single 0.2 m clean region (*L*2) shows an almost constant time of arrival for the 10 Hz oscillation, which indicated that a longer length of source region was more sensitive to the strength change in the time domain. Therefore, it can be assumed that these periodic strength changes in microphones along the spanwise direction produce a periodic directivity pattern in the time domain, which occurs in spanwise configurations with long enough source regions. In addition, the tripping regions inside *L*6 and *L*8 produce *L*6*T*2 and *L*8*T*4 with a more uniform source strength distribution and a stronger periodic directivity pattern along the spanwise direction.

As a result, this periodic directivity pattern for the low-frequency oscillation contributes to periodic source localization within a 10 Hz period time. By selecting a range of 0.2 s for the two period times at 10 Hz, the wavelet-based beamforming method produces the transient source localization for different spanwise configurations in Figure 15. For a compact single 0.2 m clean source region, *L*2 shows a consistent pattern with the single microphone, resulting in a periodic strength change without spatial change. For an increased length of source region from *L*4 to *L*8, an unsteady change along the spanwise direction can be found more and more clearly. For *L*6*T*2 and *L*8*T*4, transient maps indicate sound sources in the tripping regions. Although it should be partially due to the Rayleigh limit, which is mentioned in previous time-average discussions, the periodic switch between two types of source distribution should be greatly influenced by the periodic directivity pattern along the spanwise direction. The significant time delays along the spanwise direction directly

change the transient strength from different microphones in Equation (1) to produce source strength distribution maps.

Furthermore, by using source power integration methods [52,53], transient total strength as the summed SPL along the spanwise direction was produced, which highlighted the spanwise difference in the time domains. As shown in Figure 16, the consecutive spanwise configuration from *L*2 to *L*8 tends to show a consecutive change along the spanwise direction, while for *L*6*T*2 and *L*8*T*4, an interruption between two 0.2 sources region was found, which was unlike the time-average results in Figure 8. It should be noted that although the unsteady intermittent patterns prevail in source regions with a large spanwise length, periodic strength change at 10 Hz always exists in Figures 12 and 16. Since the strong low-frequency oscillation is inherent due to the wind tunnel buffeting, it can be assumed that a periodic vortical structure is strong enough to dominate the acoustic feedback loop, which contributes to the current spanwise periodic directivity pattern in Figure 14.

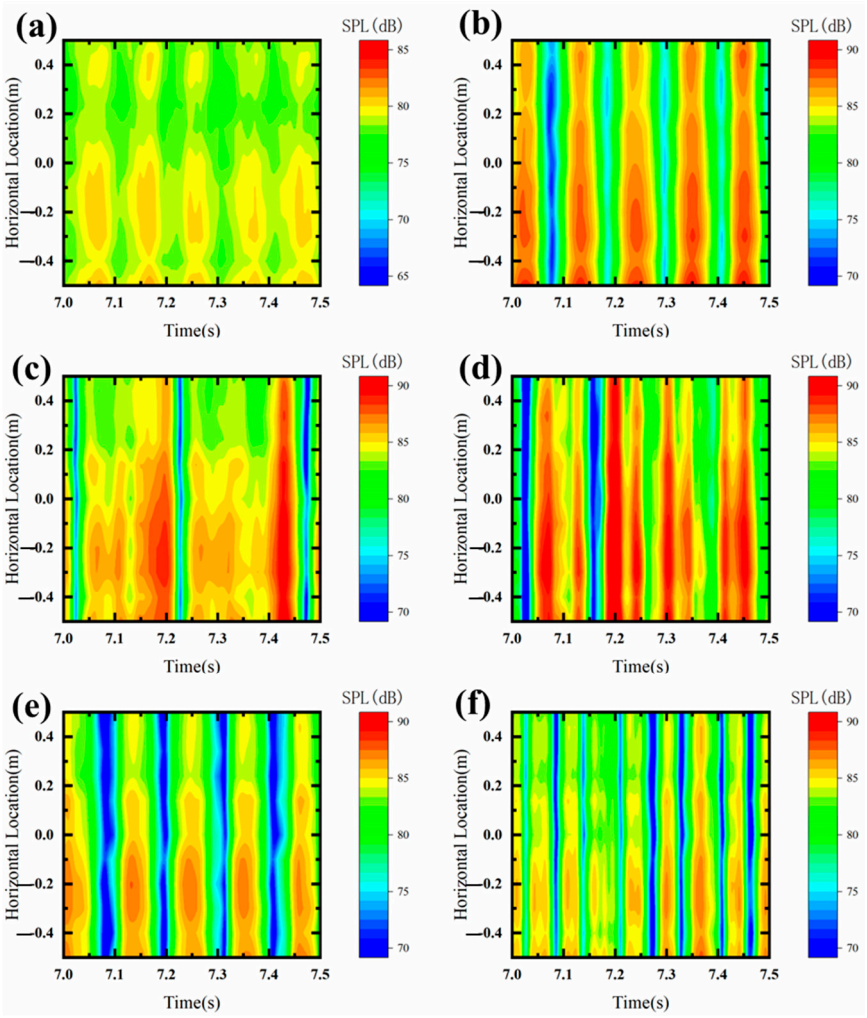


Figure 13. The contour maps of sound pressure level (SPL) for each microphone in the horizontal line in time domain for different spanwise configurations. SPL is summed around the tonal frequency in a 1/3 octave. The incoming velocity is 24 m/s. (**a**) *L*2; (**b**) *L*4; (**c**) *L*6; (**d**) *L*8; (**e**) *L*6*T*2; (**f**) *L*8*T*4.

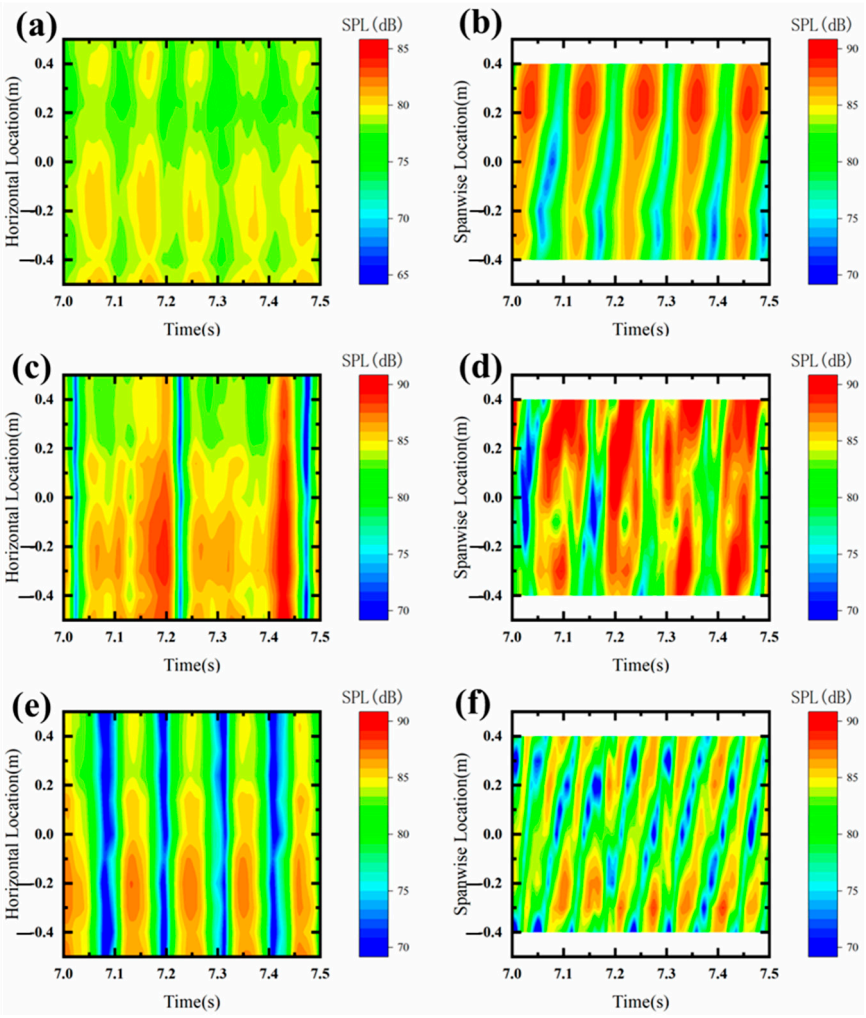
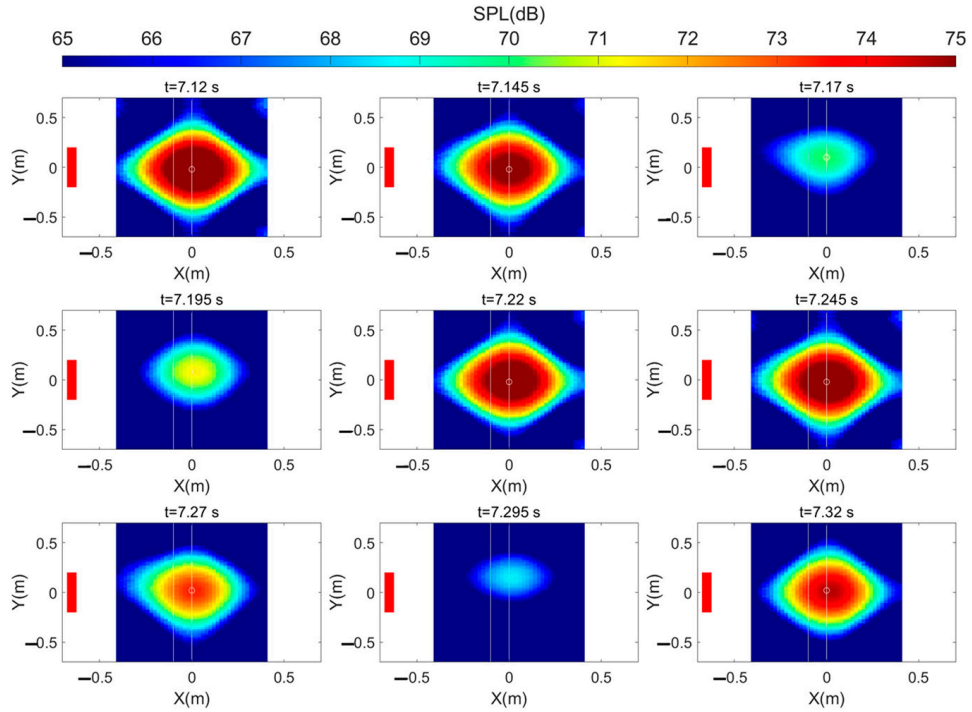
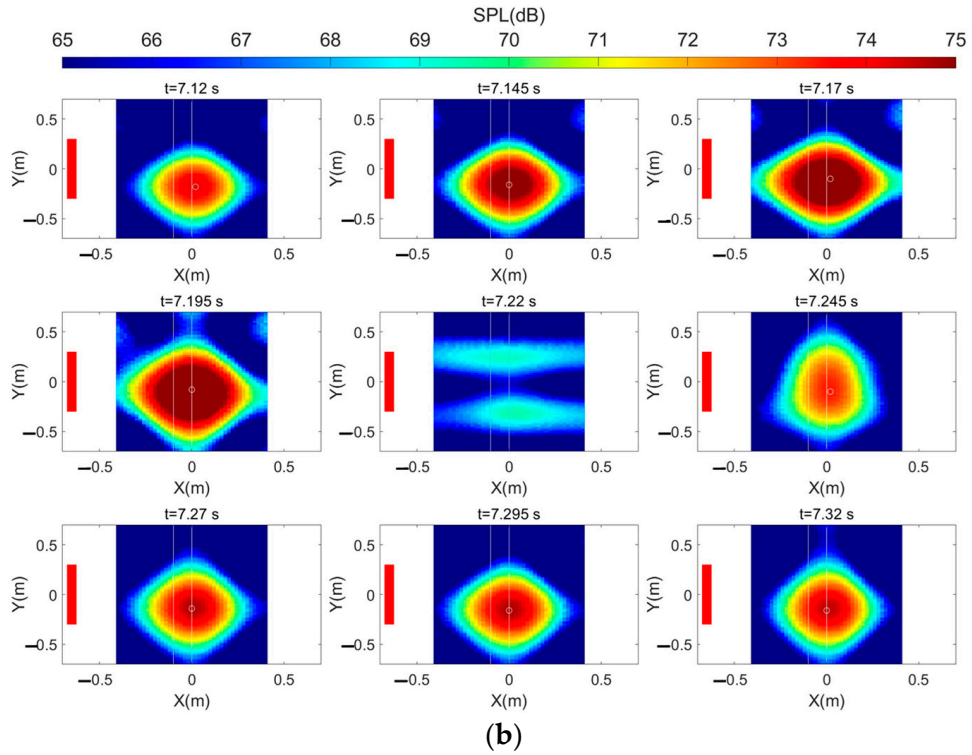


Figure 14. The contour maps of sound pressure level (SPL) for each microphone in the spanwise line in time domain for different spanwise configurations. SPL is summed around the tonal frequency in a 1/3 octave. The incoming velocity is 24 m/s. (**a**) *L*2; (**b**) *L*4; (**c**) *L*6; (**d**) *L*8; (**e**) *L*6*T*2; (**f**) *L*8*T*4.

Based on the above results, the strength influence can be changed to add weights in Equation (1) for different microphones. Considering the periodic directivity pattern in the time domain along the spanwise direction, weight coefficients are added to decrease the influence of consistent horizontal microphones. As a result, the transient source localization in Figure 17 for *L*6*T*2 and *L*8*T*4 reduces the strength change between the consecutive source and separated sources. This conclusion can also be applied to time-average source localization. As shown in Figure 18, the weighted source localization tends to increase the spanwise distribution along the spanwise direction between two source regions. Therefore, it can be concluded that the 10 Hz oscillation is critical in changing the roles of different microphones in source localizations, which should be paid attention in experiments.

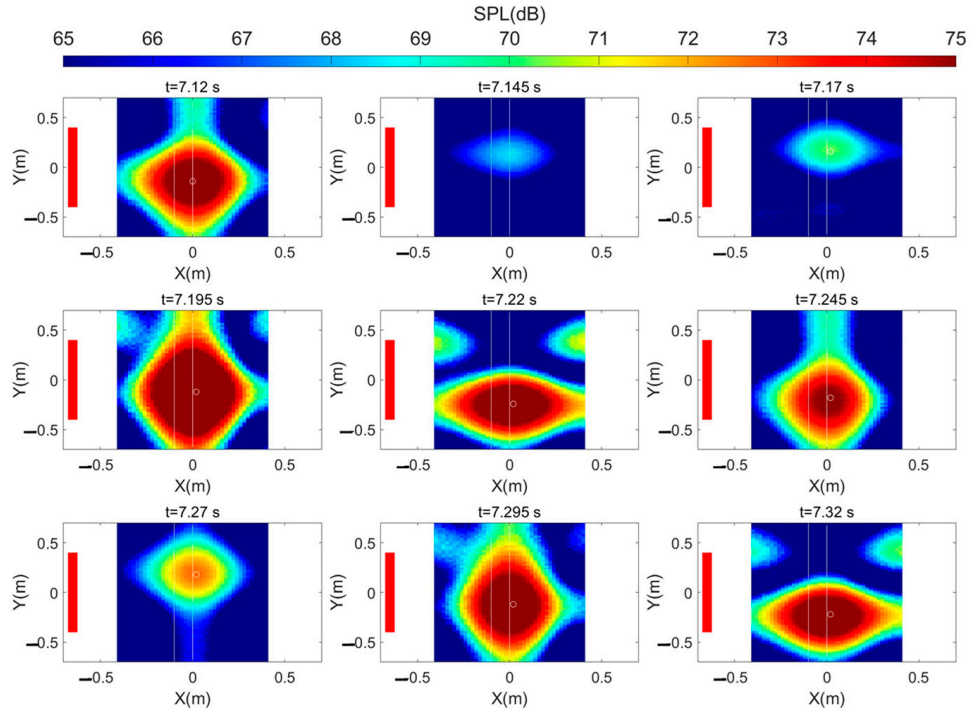


(**a**)

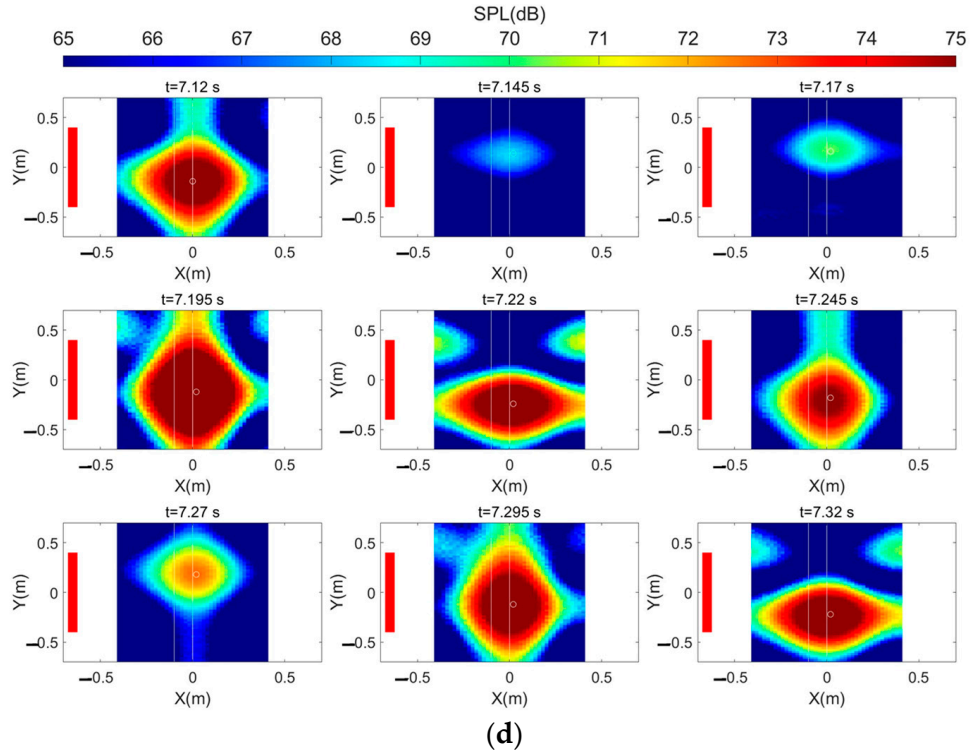


(**b**)

Figure 15. *Cont*.



(**c**)



(**d**)

Figure 15. *Cont*.

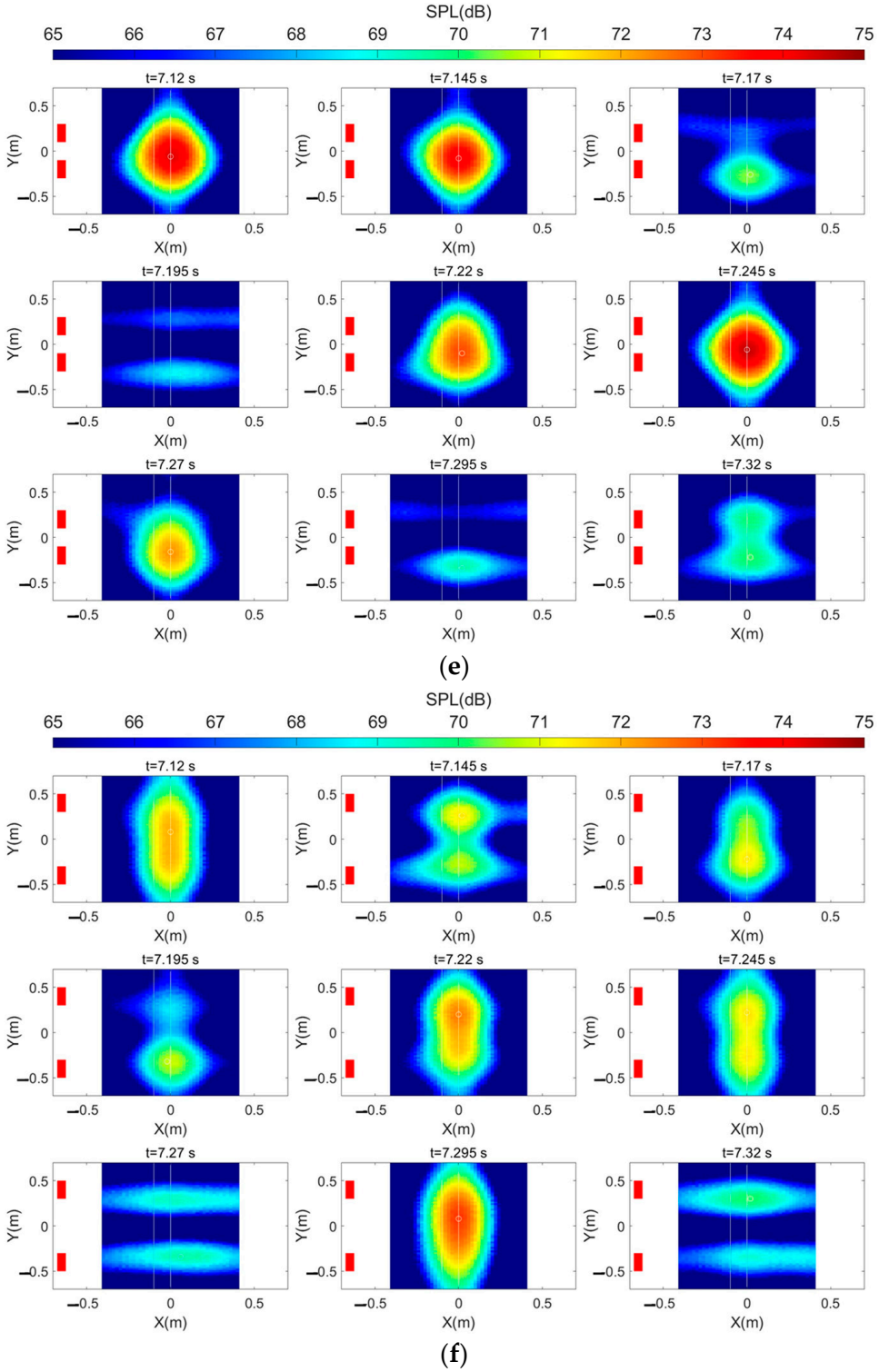


Figure 15. The transient wavelet-based results at 24 m/s for different spanwise configurations. The columns from the left and rows from the bottom are the transient wavelet-based imaging results from 7.12 s to 7.32 s, which indicate two periods at 10 Hz. (**a**) *L*2; (**b**) *L*4; (**c**) *L*6; (**d**) *L*8; (**e**) *L*6*T*2; (**f**) *L*8*T*4. The unfilled white cycles indicate the positions of maximum values.

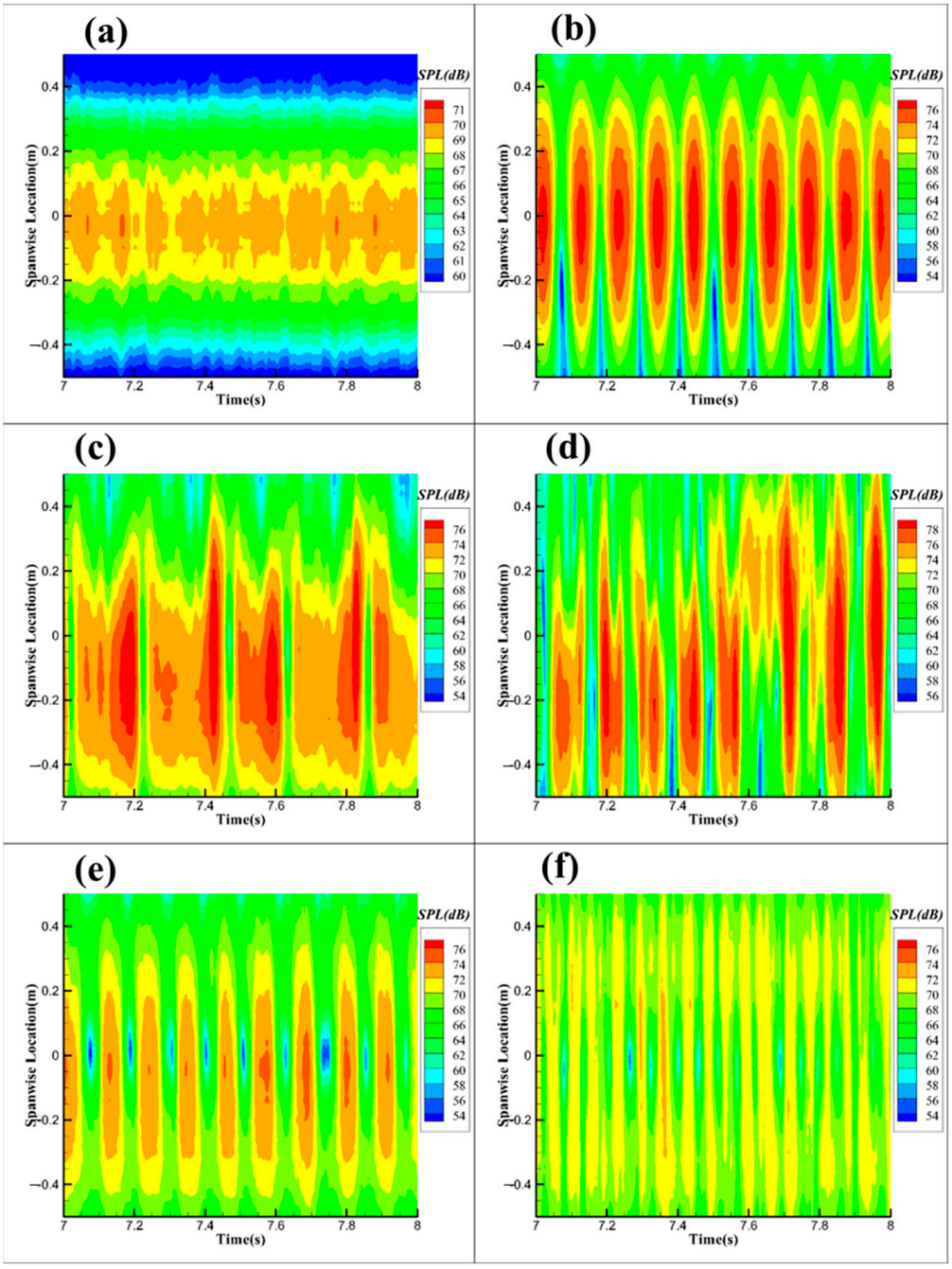


Figure 16. The summed SPL of wavelet-based beamforming results at different spanwise locations near the trailing edge in the time and spatial domain. (**a**) *L*2; (**b**) *L*4; (**c**) *L*6; (**d**) *L*8; (**e**) *L*6*T*2; (**f**) *L*8*T*4.

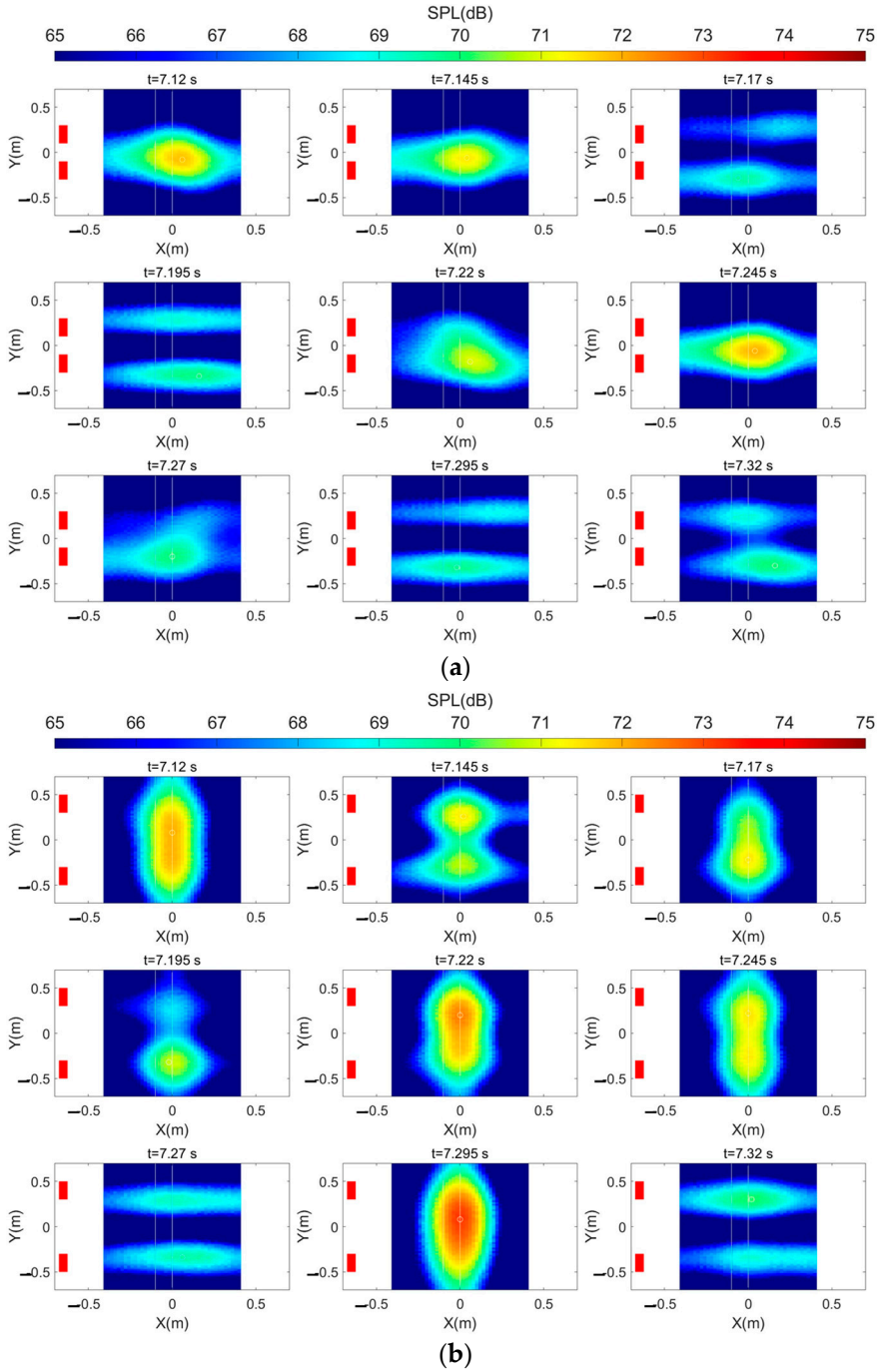


Figure 17. The weighted transient wavelet-based results at 24 m/s for different spanwise configurations. The columns from the left and rows from the bottom are the transient wavelet-based imaging results from 7.12 s to 7.32 s, which indicate two periods at 10 Hz. (**a**) *L6T2*; (**b**) *L8T4*. The unfilled white cycles indicate the positions of maximum values.

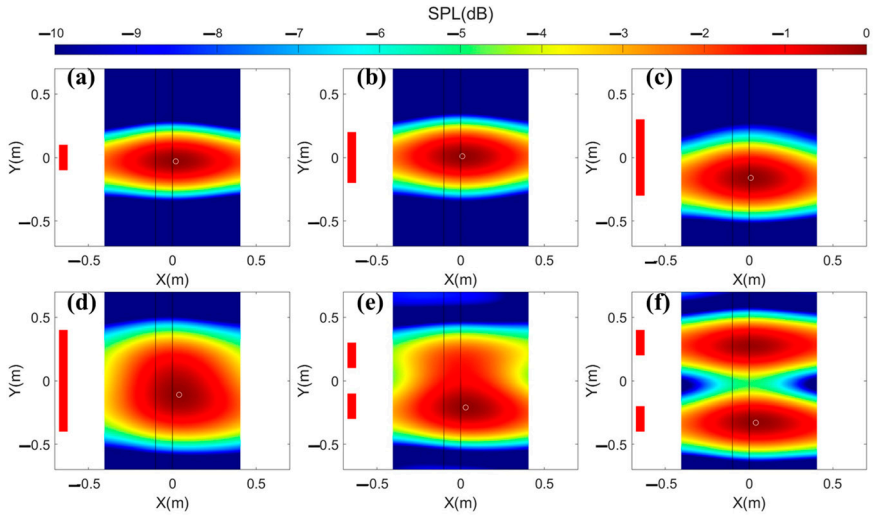


Figure 18. The weighted time-average source localization of different source regions along the spanwise location at 24 m/s according to the 21-channel cross-shaped microphone array. (**a**) *L*2; (**b**) *L*4; (**c**) *L*6; (**d**) *L*8; (**e**) *L*6*T*2; (**f**) *L*8*T*4. The unfilled white cycles indicate the positions of maximum values.

4. Conclusions

In this paper, an investigation of the low-frequency oscillation on the trailing-edge tonal noise was carried out. Inspired by previous experiments for high-frequency oscillations from unsteady coherent flows, the present study aimed to figure out the influence of low-frequency oscillations from the wind tunnels. By using tripping tapes to diminish the local sources, configurations for symmetry spatial distributions of source regions were generated to check the noise characteristics. Periodic strength change was focused upon by continuous wavelet analysis to reveal the spatial difference between microphones at different locations.

In wind tunnel experiments, the NACA0012 airfoil trailing-edge tonal noise was measured by two microphone arrays that were used to analyze the time-average and transient characteristics. For the time-average patterns, a consistent source strength distribution in a 0.2 m source region along the spanwise direction was validated by a 64-channel spiraled microphone array. And a symmetric source strength distribution was found for symmetric spanwise configurations by a 21-channel cross-shaped array. The impact of a low-frequency oscillation on the time-average results was generally insignificant, except for on the side secondary tones due to amplitude modulation.

In contrast, for the transient analysis by continuous wavelet methods, a periodic strength change pattern around the dominant tone emerges from each microphone's result. The increasing length of source regions without tripping from *L*2 to *L*8 produced more intermittent broadband patterns in the time domain. Meanwhile, based on the simultaneous transient wavelet coefficients, a significantly large delay of time for the 10 Hz oscillation occurs between microphones along the spanwise direction rather than the horizontal direction. The delay time is almost 0.1 s, which is much larger than the maximum propagating delay time between microphones of 0.02 s. Therefore, a significant periodic directivity pattern was found along the spanwise direction. As a result, the transient source localization caused by the wavelet-based beamforming method contributes to a switching pattern between the two types of results. One of the results is similar to the time-average results as a consecutive line source strength distribution, while the other separates the sources in different source regions better than the Rayleigh limit. Hence, low-frequency oscillations play a role in changing the transient spatial directivity of sources, which was quite interesting and few discussions had been undertaken before.

Moreover, for microphone arrays in transient source localization, the time delay as a shift of phase in the frequency-time domains greatly influences the results of wavelet-based beamforming methods, which produces a switching pattern between different spatial dis-

tributions. Therefore, based on the weighted results, to decrease the influence of horizontal microphones in the symmetrical line, it can be assumed that a low-frequency oscillation increases the spanwise complexity in transient source localization even for symmetric spanwise source regions. However, since the low-frequency oscillation is inherent due to the wind tunnel buffeting, a periodic pattern should exist, which contributes to the current results in the spatial domain. Since this pattern was greatly involved with low-frequency oscillations, the response from different airfoils or even different regions within a three-dimensional wing model might be considered in experiments. Furthermore, the same NACA0012 airfoil in different wind tunnels might possess different transient noise spectra and these spectra were highly related to the location of sources due to this periodic directivity pattern. However, since only NACA0012 as a 0.1 m chord length symmetric airfoil is involved in the current study with different spanwise configurations, there might be other patterns for unsymmetric airfoils. Future investigations should be conducted for other different airfoils. In addition, artificial low-frequency oscillations could be generated to further check the effects of the oscillations at different frequencies.

Considering that all these complicated patterns exist with only side secondary tones being involved in this experiment, the primary secondary tones with a much higher frequency interval should be handled with more caution. For further investigations of trailing-edge tonal noise, the current study indicates that transient analysis could be greatly influenced by external disturbances in the wind tunnel, which partially explains the difference between experiments and simulations. Noise measurement of different airfoils should be performed with multiple microphones along the spanwise direction to check if the periodic directivity pattern exists. Meanwhile, since it was confirmed that the source's directivity might change dramatically in the time domain due to wind tunnel buffeting, it should be similar for other external disturbances in a low frequency in the real environment. As a result, the environment in applications should be considered in the design of airfoils. Supplementary experiments should be conducted to investigate the potential influence of low-frequency oscillations.

Author Contributions: Conceptualization, Z.S. and H.G.; data curation, Z.S.; formal analysis, Z.S.; funding acquisition, H.G., Y.S. and S.J.; investigation, Z.S.; methodology, Z.S.; project administration, H.G.; resources, P.L., H.G., Y.S. and S.J.; software, Z.S.; supervision, P.L.; validation, H.G.; visualization, Z.S.; writing—original draft, Z.S.; writing—review and editing, Z.S., P.L. and H.G. All authors have read and agreed to the published version of the manuscript.

Funding: This research was funded by the National Natural Science Foundation of China (No. 12072016), National Key R&D Program of China (No. 2022YFB2602000), Research Fund of the Key Laboratory of Aerodynamic Noise Control (No. ANCL20220303), and the Fundamental Research Funds for the Central Universities.

Data Availability Statement: Some or all of the data, models, or codes that support the findings of this study are available from the corresponding author upon reasonable request.

Acknowledgments: Thanks to all team members for participating in the experiments and analyzing process.

Conflicts of Interest: The authors declare no conflicts of interest. The funders had no role in the design of the study; in the collection, analyses or interpretation of data; in the writing of the manuscript; or in the decision to publish the results.

References

1. Dobrzynski, W. Almost 40 Years of Airframe Noise Research: What Did We Achieve? *J. Aircr.* **2010**, *47*, 353–367. [CrossRef]
2. Grande, E.; Ragni, D.; Avallone, F.; Casalino, D. Laminar Separation Bubble Noise on a Propeller Operating at Low Reynolds Numbers. *AIAA J.* **2022**, *60*, 5324–5335. [CrossRef]
3. Zhang, Y.; Avallone, F.; Watson, S. Wind Turbine Blade Trailing Edge Crack Detection Based on Airfoil Aerodynamic Noise: An Experimental Study. *Appl. Acoust.* **2022**, *191*, 108668. [CrossRef]
4. Brooks, F.; Stuart, D.; Marcolini, A. *Airfoil Self-Noise and Prediction*; NASA Reference Publication 1218; NASA: Washington, DC, USA, 1989.
5. Lee, S. The Effect of Airfoil Shape on Trailing Edge Noise. *J. Theor. Comp. Acout.* **2019**, *27*, 1850020. [CrossRef]

6. Liu, C.; Lee, S. Parametric Airfoil Design and Sensitivity Analysis for Turbulent Boundary-Layer Trailing-Edge Noise Reduction. *AIAA J.* **2022**, *60*, 2324–2341. [CrossRef]
7. Paterson, R.W.; Vogt, P.G.; Fink, M.R.; Munch, C.L. Vortex Noise of Isolated Airfoils. *J. Aircr.* **1973**, *10*, 296–302. [CrossRef]
8. Tam, C.K.W. Discrete Tones of Isolated Airfoils. *J. Acoust. Soc. Am.* **1974**, 55. [CrossRef]
9. Fink, M.R. Prediction of Airfoil Tone Frequencies. *J. Aircr.* **1975**, *12*, 118–120. [CrossRef]
10. Longhouse, R.E. Vortex Shedding Noise of Low Tip Speed, Axial Flow Fans. *J. Sound Vib.* **1977**, *53*, 25–46. [CrossRef]
11. Arbey, H.; Bataille, J. Noise Generated by Airfoil Profiles Placed in a Uniform Laminar Flow. *J. Fluid Mech.* **1983**, *134*, 33–47. [CrossRef]
12. Nash, E.C.; Lowson, M.V.; McALPINE, A. Boundary-Layer Instability Noise on Aerofoils. *J. Fluid Mech.* **1999**, *382*, 27–61. [CrossRef]
13. Desquesnes, G.; Terracol, M.; Sagaut, P. Numerical Investigation of the Tone Noise Mechanism over Laminar Airfoils. *J. Fluid Mech.* **2007**, *591*, 155–182. [CrossRef]
14. Arcondoulis, E.J.G.; Doolan, C.J.; Zander, A.C.; Brooks, L.A. A Review of Trailing Edge Noise Generated by Airfoils at Low To Moderate Reynolds Number. *Acoust. Aust.* **2010**, *3*, 135–139.
15. Pröbsting, S.; Serpieri, J.; Scarano, F. Experimental Investigation of Aerofoil Tonal Noise Generation. *J. Fluid Mech.* **2014**, *747*, 656–687. [CrossRef]
16. Pröbsting, S.; Scarano, F.; Morris, S.C. Regimes of Tonal Noise on an Airfoil at Moderate Reynolds Number. *J. Fluid Mech.* **2015**, *780*, 407–438. [CrossRef]
17. Pröbsting, S.; Yarusevych, S. Laminar Separation Bubble Development on an Airfoil Emitting Tonal Noise. *J. Fluid Mech.* **2015**, *780*, 167–191. [CrossRef]
18. Padois, T.; Laffay, P.; Idier, A.; Moreau, S. Tonal Noise of a Controlled-Diffusion Airfoil at Low Angle of Attack and Reynolds Number. *J. Acoust. Soc. Am.* **2016**, *140*, EL113–EL118. [CrossRef]
19. Yakhina, G.; Roger, M.; Moreau, S.; Nguyen, L.; Golubev, V. Experimental and Analytical Investigation of the Tonal Trailing-Edge Noise Radiated by Low Reynolds Number Aerofoils. *Acoustics* **2020**, *2*, 293–329. [CrossRef]
20. Golubev, V. Recent Advances in Acoustics of Transitional Airfoils with Feedback-Loop Interactions: A Review. *Appl. Sci.* **2021**, *11*, 1057. [CrossRef]
21. Yang, Y.; Pröbsting, S.; Li, P.; Liu, Y.; Li, Y. A Secondary Modulation Mechanism for Aerofoil Tonal Self-Noise Generation. *J. Fluid Mech.* **2022**, *943*, A13. [CrossRef]
22. Yu, J.; Chen, W.; Zhou, T.; Lee, C.; Huang, X. Transient Analysis of Trailing Edge Noise Assisted by Wavelet-Based Beamforming and Flow Visualisation. *J. Sound Vib.* **2022**, *526*, 116751. [CrossRef]
23. Ricciardi, T.R.; Wolf, W.R.; Taira, K. Transition, Intermittency and Phase Interference Effects in Airfoil Secondary Tones and Acoustic Feedback Loop. *J. Fluid Mech.* **2022**, *937*, A23. [CrossRef]
24. Ricciardi, T.R.; Wolf, W.R. Switch of Tonal Noise Generation Mechanisms in Airfoil Transitional Flows. *Phys. Rev. Fluids* **2022**, *7*, 084701. [CrossRef]
25. Sano, A.; Cavalieri, A.V.G.; Da Silva, A.F.C.; Wolf, W.R. On the Emergence of Secondary Tones in Airfoil Noise. *J. Fluid Mech.* **2023**, *966*, A8. [CrossRef]
26. Smith, T.A.; Klettner, C.A. Airfoil Trailing-Edge Noise and Drag Reduction at a Moderate Reynolds Number Using Wavy Geometries. *Phys. Fluids* **2022**, *34*, 117107. [CrossRef]
27. Chen, W.; Wang, X.; Xing, Y.; Wang, L.; Qiao, W. Effect of Wavy Leading Edges on Airfoil Tonal Noise. *Phys. Fluids* **2023**, *35*, 097136. [CrossRef]
28. Kojima, Y.; Skene, C.S.; Yeh, C.-A.; Taira, K.; Kameda, M. On the Origin of Quadrupole Sound from a Two-Dimensional Aerofoil Trailing Edge. *J. Fluid Mech.* **2023**, *958*, A3. [CrossRef]
29. Wang, Y.; Zuo, K.; Guo, P.; Zhao, K.; Kopiev, V.F. Experimental Investigation of Airfoil Instability Tonal Noise Reduction Using Structured Porous Trailing Edges. *Appl. Sci.* **2024**, *14*, 2992. [CrossRef]
30. Yarusevych, S.; Kotsonis, M. Steady and Transient Response of a Laminar Separation Bubble to Controlled Disturbances. *J. Fluid Mech.* **2017**, *813*, 955–990. [CrossRef]
31. Andan, A.D.; Lee, D.-J. Effect of External Acoustic Excitation on NACA0015 Discrete Tonal Noise. *Appl. Acoust.* **2018**, *141*, 374–381. [CrossRef]
32. Gelot, M.B.R.; Kim, J.W. Effect of Serrated Trailing Edges on Aerofoil Tonal Noise. *J. Fluid Mech.* **2020**, *904*, A30. [CrossRef]
33. Ahuja, K.; Massey, K.; D'Agostino, M.; Ahuja, K.; Massey, K.; D'Agostino, M. Flow/Acoustic Interactions in Open-Jet Wind Tunnels. In Proceedings of the 3rd AIAA/CEAS Aeroacoustics Conference, Atlanta, GA, USA, 12–14 May 1997; American Institute of Aeronautics and Astronautics: Reston, VA, USA, 1997.
34. Jin, L.; Deng, X.B.; Wang, X.; Gu, Y.; Liang, Y.; Lian, Z. Standing Waves in the Plenum of an Open Jet Wind Tunnel: Resonance and Self-Excited Oscillation. *AIP Adv.* **2022**, *12*, 025105. [CrossRef]
35. Jin, L.; Gu, Y.; Deng, X.B.; Sun, H.; Yue, T.; Zhang, J. Standing Wave and Its Impact on the Low-Frequency Pressure Fluctuation in an Open Jet Wind Tunnel. *J. Wind Eng. Ind. Aerodyn.* **2021**, *208*, 104413. [CrossRef]
36. Ma, R.; Li, H.; Han, S.; Wu, C.; Zhang, S.; Wang, X. Numerical Simulation of Low Frequency Oscillation in an Aeroacoustic Wind Tunnel. *J. Phys. Conf. Ser.* **2022**, *2329*, 012017. [CrossRef]

37. Sellers, W.L.; Applin, Z.T.; Molloy, J.K. *Effect of Jet Exit Vanes on Flow Pulsations in an Open-Jet Wind Tunnel*; Technical Report No. NASA-TM-86299; Langley Research Center: Hampton, VA, USA, 1985.
38. Martin, R.M.; Brooks, T.F.; Hoad, D.R. Reduction of Background Noise Induced by Wind Tunnel Jet Exit Vanes. *AIAA J.* **1985**, *23*, 1631–1632. [CrossRef]
39. von Heesen, W.; Höpfer, M. Suppression of Wind Tunnel Buffeting by Active Flow Control. *SAE Trans.* **2004**, *113*, 431–441.
40. Kudo, T.; Komatsu, Y.; Maeda, K.; Nishimura, M. Techniques for Reducing Low-Frequency Fluctuations in Aeroacoustic Wind Tunnels. *J. Environ. Eng.* **2009**, *4*, 289–301. [CrossRef]
41. Chen, W. Acoustic Receptivity in the Airfoil Boundary Layer: An Experimental Study in a Closed Wind Tunnel. *Phys. Fluids* **2023**, *35*, 043616. [CrossRef]
42. Roder, H. Amplitude, Phase, and Frequency Modulation. *Proc. IRE* **1931**, *19*, 2145–2176. [CrossRef]
43. Brandstein, M.; Ward, D. (Eds.) *Microphone Arrays: Signal Processing Techniques and Applications. Digital Signal Processing*; Springer: Berlin/Heidelberg, Germany, 2001; ISBN 978-3-642-07547-6.
44. Sanders, M.P.; Botero, L.; De Santana, L.D.; Venner, C. Airfoil Trailing Edge Noise Measurements in an Open-Jet, Hard-Wall and Kevlar-Wall Test Section: A Benchmark Exercise. In Proceedings of the AIAA AVIATION 2021 Forum, Virtual Event, 2–6 August 2021; American Institute of Aeronautics and Astronautics: Reston, VA, USA, 2021.
45. Herold, G.; Sarradj, E. Performance Analysis of Microphone Array Methods. *J. Sound Vib.* **2017**, *401*, 152–168. [CrossRef]
46. Zhou, H.; Liu, Z.; Luo, L.; Wang, M.; Song, X. An Improved Two-Stage Spherical Harmonic ESPRIT-Type Algorithm. *Symmetry* **2023**, *15*, 1607. [CrossRef]
47. Chen, W.; Huang, X. Wavelet-Based Beamforming for High-Speed Rotating Acoustic Source. *IEEE Access* **2018**, *6*, 10231–10239. [CrossRef]
48. Chen, W.; Peng, B.; Liem, R.P.; Huang, X. Experimental Study of Airfoil-Rotor Interaction Noise by Wavelet Beamforming. *J. Acoust. Soc. Am.* **2020**, *147*, 3248–3259. [CrossRef] [PubMed]
49. Chen, W.; Yang, Z.; Peng, B.; Huang, X. On Trailing Edge Noise from Propellers with Interactions to Shear Layers. *J. Sound Vib.* **2021**, *495*, 115901. [CrossRef]
50. Liu, P.; Xing, Y.; Guo, H.; Li, L. Design and Performance of a Small-Scale Aeroacoustic Wind Tunnel. *Appl. Acoust.* **2017**, *116*, 65–69. [CrossRef]
51. Merino-Martínez, R.; Sijtsma, P.; Snellen, M.; Ahlefeldt, T.; Antoni, J.; Bahr, C.J.; Blacodon, D.; Ernst, D.; Finez, A.; Funke, S.; et al. A Review of Acoustic Imaging Methods Using Phased Microphone Arrays: Part of the "Aircraft Noise Generation and Assessment" Special Issue. *CEAS Aeronaut. J.* **2019**, *10*, 197–230. [CrossRef]
52. Brooks, T.; Humphreys, W., Jr. Effect of Directional Array Size on the Measurement of Airframe Noise Components. In Proceedings of the 5th AIAA/CEAS Aeroacoustics Conference and Exhibit, Bellevue, WA, USA, 10–12 May 1999; American Institute of Aeronautics and Astronautics: Reston, VA, USA, 1999.
53. Merino-Martínez, R.; Sijtsma, P.; Carpio, A.R.; Zamponi, R.; Luesutthiviboon, S.; Malgoezar, A.M.; Snellen, M.; Schram, C.; Simons, D.G. Integration Methods for Distributed Sound Sources. *Int. J. Aeroacoustics* **2019**, *18*, 444–469. [CrossRef]

Disclaimer/Publisher's Note: The statements, opinions and data contained in all publications are solely those of the individual author(s) and contributor(s) and not of MDPI and/or the editor(s). MDPI and/or the editor(s) disclaim responsibility for any injury to people or property resulting from any ideas, methods, instructions or products referred to in the content.